ANTIOXIDANTS & REDOX SIGNALING
Volume 2, Number 3, 2000
Mary Ann Liebert, Inc.

Original Research Communication

Characterization of Human and Mouse Peroxiredoxin IV: Evidence for Inhibition by Prx-IV of Epidermal Growth Factor- and p53-Induced Reactive Oxygen Species

CHI-MING WONG,[1] ABEL C.S. CHUN,[1] K.H. KOK,[2] YUAN ZHOU,[1] PETER C.W. FUNG,[2] HSIANG-FU KUNG,[1] KUAN-TEH JEANG,[3] and DONG-YAN JIN[1,3]

ABSTRACT

The aim of this study was to identify and characterize human and mouse Prx-IV. We identified mouse peroxiredoxin IV (Prx-IV) by virtue of sequence homology to its human ortholog previously called AOE372. Mouse Prx-IV conserves an amino-terminal presequence coding for signal peptide. The amino acid sequences of mature mouse and human Prx-IV share 97.5% identity. Phylogenetic analysis demonstrates that Prx-IV is more closely related to Prx-I/-II/-III than to Prx-V/-VI. Previously, we mapped the mouse Prx-IV gene to chromosome X by analyzing two sets of multiloci genetic crosses. Here we performed further comparative analysis of mouse and human Prx-IV genomic loci. Consistent with the mouse results, human Prx-IV gene localized to chromosome Xp22.135–136, in close proximity to SAT and DXS7178. A bacterial artificial chromosome (BAC) clone containing the complete human Prx-IV locus was identified. The size of 7 exons and the sequences of the splice junctions were confirmed by PCR analysis. We conclude that mouse Prx-IV is abundantly expressed in many tissues. However, we could not detect Prx-IV in the conditioned media of NIH-3T3 and Jurkat cells. Mouse Prx-IV was specifically found in the nucleus-excluded region of cultured mouse cells. Intracellularly, overexpression of mouse Prx-IV prevented the production of reactive oxygen species induced by epidermal growth factor or p53. Taken together, mouse Prx-IV is likely a cytoplasmic or organellar peroxiredoxin involved in intracellular redox signaling. Antiox. Redox Signal. 2, 507–518.

INTRODUCTION

PEROXIREDOXINS ARE A NEW FAMILY of antioxidant enzymes abundantly found in living organisms ranging from bacteria to human (Chae *et al.*, 1994b; Jin and Jeang, 2000). Representative microbial and mammalian peroxiredoxins have been characterized as a terminal peroxidase, which reduces hydrogen peroxide and/or organic hydroperoxides using thioredoxin, tryparedoxin, glutathione, or other molecules as electron donor (Chae *et al.*, 1994a; Jin *et al.*, 1997; Kang *et al.*, 1998a,b; Montemartini *et al.*, 1998; Singh and Shichi, 1998; Fisher *et al.*, 1999). All peroxiredoxin proteins conserve a structural motif surrounding a cysteine residue, which is the peroxidatic center (Chae *et al.*, 1994b; Choi *et al.*, 1998; Hirotsu *et al.*, 1999). The ubiquity and high conservation of peroxiredoxins suggest that they may have important roles in antioxidant defense and redox signaling. Indeed, several lines of evidence

[1]Institute of Molecular Biology, The University of Hong Kong, Pokfulam, Hong Kong.
[2]Division of Medical Physics, Department of Medicine, The University of Hong Kong, Pokfulam, Hong Kong.
[3]Molecular Virology Section, Laboratory of Molecular Microbiology, National Institute of Allergy and Infectious Diseases, National Institutes of Health, Bethesda, MD 20892-0460.

support that peroxiredoxins can influence receptor signaling, protein phosphorylation, gene expression, and apoptosis (Ichimiya *et al.*, 1997; Jin *et al.*, 1997; Zhang *et al.*, 1997; Kang *et al.*, 1998b; Kowaltowski *et al.*, 1998; Araki *et al.*, 1999).

Multiple subtypes of peroxiredoxins are often found in one species. Thus, there exist three peroxiredoxins (AhpC, Tpx/scavengase p20, and BCP) in *Escherichia coli* (Chae *et al.*, 1993, 1994b, Cha *et al.*, 1995, 1996; Wan *et al.*, 1997; Zhou *et al.*, 1997; Jin and Jeang, 2000), and five (TSA1, TSA2, BCP, 1CPrx, and PMP20) in budding yeast (Chae *et al.*, 1994a; Jeong *et al.*, 1999; Lee *et al.*, 1999; Verdoucq *et al.*, 1999). As yet, six subfamilies (I–VI) have been identified in mammals (Chae *et al.*, 1994b; Frank *et al.*, 1997; Jin *et al.*, 1997; Haridas *et al.*, 1998; Kang *et al.*, 1998a,b; Lim *et al.*, 1998; Singh and Shichi, 1998; Knoops *et al.*, 1999; Kropotov *et al.*, 1999; Lyu *et al.*, 1999; Matsumoto *et al.*, 1999; Yamashita *et al.*, 1999; Zhou *et al.*, 2000). Mammalian peroxiredoxins are abundantly expressed in cells. However, different subtypes show distinct tissue distribution patterns and target to different subcellular compartments (Jin *et al.*, 1997; Kang *et al.*, 1998a,b; Montemartini *et al.*, 1998; Singh and Shichi, 1998; Araki *et al.*, 1999; Matsumoto *et al.*, 1999; Sarafian *et al.*, 1999). Thus, they may serve tissue-specific functions at restricted subcellular locations.

To understand the biological interplay between peroxiredoxins, it is imperative that one identifies and characterizes all known peroxiredoxins within each given species. Among the six currently known subtypes of peroxiredoxins in human, mouse, and rat, mouse Prx-IV is the only one that has not been identified. In addition, there is a discrepancy in the literature regarding the subcellular localization, secretion, and biological functions of human and rat Prx-IV (Jin *et al.*, 1997; Haridas *et al.*, 1998; Matsumoto *et al.*, 1999). Here, we have cloned a full-length mouse Prx-IV cDNA through a search for the mouse ortholog of the newly identified human Prx-IV, previously known as AOE372 (Jin *et al.*, 1997). We performed phylogenetic analysis of mammalian peroxiredoxins and comparative analysis of mouse and human Prx-IV genomic loci. We also assessed the expression profiles, subcellular localization, and secretion of mouse Prx-IV. Finally, we showed that mouse Prx-IV is a functional intracellular antioxidant enzyme.

MATERIALS AND METHODS

Materials

The expressed sequence tag (EST) cDNA clone (I.M.A.G.E. Consortium clone 367356) encoding mouse Prx-IV was from the American Type Culture Collections (Manassas, VA). The mammalian expression plasmid for wild-type human p53 (pp53; a gift from B. Vogelstein, Johns Hopkins University Oncology Center, Baltimore, Maryland) was described previously (Kern *et al.*, 1991). Plasmid pSVP4 was constructed by inserting the mouse Prx-IV cDNA (coding for amino acids 1–274, including the putative signal peptide) into a previously described (Jin *et al.*, 1998) eukaryotic expression vector with SV40 early promoter and enhancers. The expression vector for β-galactosidase (pSV-Gal) was purchased from Promega (Madison, WI). Human genomic DNA from blood was from Novagen (Madison, WI). EGF was from Life Technologies (Rockville, MD).

Sequence analysis

Double-stranded mouse Prx-IV cDNA was sequenced on both strands by the dideoxy termination method using Sequenase 2.0 (Amersham, Piscataway, NJ). Multiple alignment of Prx-IV protein sequences was generated with programs in the Genetics Computer Group software package (Version 10.0; GCG, Inc., Madison, Wisconsin). Presentation of the alignment was modified using the BOXSHADE program (Version 3.21; http://www.ch.embnet.org). Phylogenetic analysis was based on the PHYLIP software package Version 3.573 (Felsenstein, 1996). Prediction of TATA box was assisted by the TSSG/TSSW (available on the Sanger Center server; http://genomic.sanger.ac.uk) and the TFSEARCH (developed by Yutaka Akiyama; http://www.rwcp.or.jp) programs.

Chromosomal mapping

The nucleotide sequence (GenBank AC005867) of the bacterial artificial chromosome (BAC) clone GSHB-567I1 previously mapped to human chromosome Xp22.135–136 was used for physical alignment of human Prx-IV. The flanking markers are SAT and DXS7178. The sequence and mapping data were produced by the Baylor College of Medicine Human Genome Sequencing Center (http://www.hgsc.bcm.tmc.edu).

Northern and Western blot analysis

The mouse multiple tissue Northern blot (CLONTECH, Palo Alto, California) was probed with an ~1-kb ^{32}P-labeled *Xho*I–*Hind*III fragment of mouse Prx-IV using manufactuer's protocol.

Proteins from total extracts of cultured cells were solubilized in sodium dodecyl sulfate (SDS) gel loading buffer (60 m*M* Tris base, 2% SDS, 10% glycerol, 5% 2-mercaptoethanol). Concentration of the culture medium was achieved by ultrafiltration through a Centricon-10 concentrator (Amicon, Bedford, MA). Cell samples containing 20 μg of protein and medium samples concentrated from 3 ml of culture medium were separated by 12% SDS- polyacrylamide gel electrophoresis (PAGE), and electroblotted onto Immobilon-P membranes (Millipore, Bedford, MA) using a Millipore semidry transfer apparatus. Immunodetection was performed with a rabbit antiserum (372-1) raised against a keyhole limpet hemocyanin-conjugated synthetic Prx-IV peptide, whose sequence is indicated in Fig. 2 (below). The blot was detected using chemiluminescence (Western-Light, Tropix, Bedford, MA) using goat anti-rabbit antibody conjugated to alkaline phosphatase. The primary and secondary antibodies were diluted to 1:1,000 and 1:10,000, respectively. NIH-3T3 cells were transfected using the calcium phosphate method, and transfection of Jurkat cells was achieved by electroporation.

Confocal microscopy

Confocal laser-scanning immunofluorescence microscopy was performed as described previously (Jin *et al.*, 1997). The 372-1 rabbit anti-Prx-IV antiserum described above was used at 1:60 dilution. An argon ion laser with an emission line at 488 nm was used to excite fluorescein dye conjugated to a goat anti-rabbit IgG secondary antibody (1:50 dilution).

ROS detection

Intracellular reactive oxygen species (ROS) were measured by confocal fluorescence microscopy using the dye 2′, 7′-dichlorodihydrofluorescein diacetate (Molecular Probes, Inc., Eugene, OR), which is oxidized by biological oxidants to give the highly fluorescent 2′,7′-dichlorofluorescein (DCF). Cultured A431 and NIH-3T3 cells were harvested into medium containing 0.2% fetal calf serum (FCS) and 10 μM fluorescent dye. After incubation for 8 min, 30 cells from each group were measured for fluorescent intensity under a confocal laser-scanning microscope (Carl Zeiss, Esslingen, Germany). DCF was excited by an argon ion laser with an emission line at 488 nm. Cells were transfected with the calcium phosphate method. The p53-expressing cells were recognized by staining with a mouse monoclonal anti-p53 antibody (DO-1; Santa Cruz Biotech., Santa Cruz, CA). A helium-neon laser with an emission line at 633 nm was used to excite Cyanine 5.18 conjugated to the secondary antibody (goat anti-mouse IgG). Likewise, β-galactosidase-expressing cells were selected by staining with a mouse monoclonal anti-β-galactosidase antibody (GAL-13, Sigma, St. Louis, MO).

RESULTS

Chromosomal mapping of mouse and human Prx-IV genes

Emerging evidence supports the importance of peroxiredoxins in various aspects of redox signaling (Jin and Jeang, 2000). Currently, six subfamilies of mammalian peroxiredoxins have been identified. To understand the human Prx-IV gene better, we located it on the human genome by sequence alignment. Using cDNA information, we identified one genomic clone that contained the complete coding and non-

coding regions of human Prx-IV. This was a BAC clone from the Genome Systems library I. The clone identification number is GSHB-567I1 (GenBank AC005867). This clone maps to Xp22.135–136. It is positive for DXS7178 and SAT markers. The distance between Prx-IV and SAT is within 100 kb. This map location was confirmed by polymerase chain reaction (PCR) analysis.

Approximately 46 kb of assembled sequence from BAC clone GSHB-567I1 was obtained. The human Prx-IV gene spans approximately 20 kb. The sizes of all exons (Fig. 1A) and introns (Fig. 1B) were independently confirmed by PCR analysis of human genomic DNA. The sequences of all splice junctions (Fig. 1B) and of the 5′ upstream region (Fig. 1C) were verified by direct sequencing of PCR products. The human Prx-IV locus contains at least 7 exons. The 6 introns follow the usual GT/AG rule (Fig. 1B). The exons vary in size from 35 to 284 bp (Fig. 1A). A putative TATA box (underlined) was identified in the 5′-flanking region. We provided an accurate genomic definition of the human Prx-IV locus. Our data are generally consistent with the chromosomal map location of human Prx-IV, which was reported to be Xp21–22.1 (Haridas *et al.*, 1998) or Xp21.3 (FISH analysis; Matsumoto *et al.*, 1999).

Molecular cloning of mouse Prx-IV

Previously, we defined the chromosomal map location of Prx-IV gene in the mouse genome (Lyu *et al.*, 1999). A mouse Prx-IV probe identified restriction site polymorphic *Pvu* II fragments of 9.2 and 11.5 kb in NFS/N and *Mus spretus*, respectively. These fragments were mapped to mouse chromosome X with the following gene order and distances: Htr1c-2.3 ± 1.6-Prdx4-1.6 ± 1.6-Grpr. The murine results are generally consistent with the current mapping data from human. The recent identification of human Prx-IV, provisionally called AOE372 (Jin *et al.*, 1997), provided us with the information used to isolate a mouse ortholog. Several ESTs cloned from the Soares mouse (strain C57BL/6J) embryo (NbME13.5-14.5) cDNA library (GenBank AA003828, W53950, W98895) were identified in a BLAST homology search against the full-length human Prx-IV sequence. One of these EST clones (GenBank W53950; IMAGE Consortium clone 367356) containing putative initiating ATG was obtained, and its complete nucleotide sequence was determined. Based on sequence data we assembled an apparently complete cDNA (~1 kb) encoding mouse Prx-IV (Fig. 2). This sequence was deposited into GenBank under accession number U96746 (deposited, April, 1997). At time of deposition, there was no other sequence available in the database for mouse Prv-IV.

Mouse Prx-IV is predicted to be a 274-amino-acid polypeptide. This size is comparable to the human ortholog. A poly(A) tail is present at the 3′ terminus of the cDNA. Mouse and human Prx-IV share more than 89% identical amino acids (Fig. 3A). Notably, about 75% of the nucleotide changes between mouse and human Prx-IV cDNAs are synonymous substitutions. Thus, evolution of Prx-IV genes preserves protein-encoding functions. The primary amino acid sequence (Figs. 2 and 3A) and the hydropathy plot (data not shown) of mouse Prx-IV confirmed the existence of an amino-terminal signal peptide. Interestingly, this presequence is the most diverged portion between mouse, rat, and human Prx-IV (Fig. 3A). Excluding this part of the protein, the mature Prx-IV polypeptides are extremely well conserved. Hence, mature mouse and human Prx-IV share 97.5% amino acid identity.

We constructed a phylogenetic tree for representative members of mammalian peroxiredoxins (Fig. 3B). The tree clearly classifies the currently known peroxiredoxins into six subfamilies. Prx-IV forms a separate grouping in this tree, with strong bootstrap support (100%). Notably, Prx-I, Prx-II, Prx-III, and Prx-IV are closer to each other than to Prx-V or Prx-VI. Thus, the former group of proteins may have separated first from Prx-V and Prx-VI at an earlier time and then subsequently diverged into the four subfamilies (Prx-I, Prx-II, Prx-III, and Prx-IV).

Expression of mouse Prx-IV mRNA

The availability of a novel mouse Prx-IV cDNA prompted us to examine the expression pattern of Prx-IV mRNA in mouse tissues by

A)

Exon	1	2	3	4	5	6	7
Size (bp)	284	118	117	121	131	35	113

B)

Exon	5' splice site (exon/intron)	3' splice site (intron/exon)	Intron size (kb)
1-2	AAAGCGAAGAgtaggtggtg	tctttcttagTTTCCAAGCC	3.7
2-3	CACTTGATTTgtaagtaata	tacctttcagCACATTTGTG	3.3
3-4	ATTTGGCCTGgtcagtatct	tttgttacagGATTAATACC	4.0
4-5	ACACTCTTAGgtacctttca	tgttttacagAGGTCTCTTC	3.1
5-6	CACGGAGAAGgtacctctcc	tttgttttagTCTGCCCTGC	1.1
6-7	TAGTGAAACAgtaagtatat	gttttaacagATAATCCCAG	2.6

C)

ggaagaaataggtgtgaaggatgagaaggcctacaacagtgctgagggcgcgaggccagtcacctgcgaagttttgtgtacaagatgggcccagaagg
atgaacagggtctaaaacagtgctgagggtgggagtgcagaagatcggtcacaagtgacgacacaaggtggtcttagtccagttggtggacgctcggtgg
cctgggcctgcccccagtacgcagacgcacacggcaggttgcagcggcaagcggggcggtgcccacggcggggagatgggtggggagggcaggg
aaaaggccaggggttgggtgatggggtaattgtcagaaaaaggaacaacactgctgggagagttttctggtaacttttcaagtcttcatttaaattaaaaaaaa
aaaagctgtctttgaaacaatagattaggtcactaaaaactgcctgtacgcccttgcatgctggaggaaagtaaatggttagacctaccctccctaagtttttcc
aggacttaaaagagctgcaagtagtgcagatcatggccccgttcacacaaatcacttcaagaaaaaaaattagtaaatgtctattagatcttgaaacttattcct
gtctatctggaacttggtaacctctgaccaacaactaagtccccattccttccctctcgcctcgtcttccctacttcccaacctctggtaagcagcagggtaaata
cagtcaataataatgtatatttcaaaatgaataagagtaaatttgaaatgtctcaccataaaagtcataggtaaacaaggcgatggataagttaatgtgatgtaat
catcccacattggatacatatttcaaaaaatcacattgcatcccacgaatgtatacaattatgatttgtcaagtaaatataatttttaaaaacgttaagtgacttttaa
aaagcttattagaagtataaaatgcaagccattcacaagcatataggttagattccgcttgtgaggggcttgtgtgcagtggtgaggctttgtggaagagatgg
acgtggaaagatgtctaaaacagcgcggaggtcaggaggccttgtcgctgccttcacagagttgggcaacgctcccggtcctggtcagccgcgggacgc
aggcgcaaatgcaggcttgggatgggggaggtgcggccggcgcccacgtggcggggcggggagcagataggggggggtaggggggaggagctggtc
tcgcgaggccgcgccccggttcgcgcgggcgtcgtgcacgcggttgtagctgcccggcggcggcagaaGCGGCGCTCGCGCCAAGG
GACGTGTTTCTGCGCTCGC

FIG. 1. Characterization of human Prx-IV genomic sequences. (**A**) Sizes of exons. (**B**) Splice junctions and sizes of introns. Exon sequences are in uppercase and introns are in lower case. Underlined are splice donor and acceptor consensus dinucleotides. (**C**) Sequence of 5′-flanking region in the human Prx-IV gene. Exons are in uppercase and a TATA box was underlined.

Northern blot analysis (Fig. 4). The Prx-IV probe detected a single transcript of about 1.1 kb. Also shown in the lower panel are the signals for the 2.0-kb β-actin mRNA from the same blot after reprobing with a β-actin cDNA. The β-actin bands provide normalization for the amount of mRNAs loaded into the different lanes. Prx-IV was ubiquitously expressed in all mouse tissues tested. These tissues included heart, brain, spleen, lung, liver, (skeletal) muscle, kidney, and testis. Prx-IV was most strongly expressed in heart, (skeletal) muscle, and testis mRNAs.

Expression and subcellular localization of mouse Prx-IV protein

Next, we raised specific antibody against a synthetic Prx-IV peptide to examine the expression of Prx-IV protein in the two mouse cell

```
   1   GA ATT CGG CAC GAG GGC GCG GTC TCC AGC GCG CGT TTT AGC TGG CTG      47

  48  CCT GGC GGA GGG GAC TCT GTT CTT TAC AGA GGG ACG TGT TTT CGC GCT      95

  96  TGC TTG GTC ATG GAG GCG CGG TCC AAG CTG CTG GAC GGG ACC ACG GCG     143
   1              Met Glu Ala Arg Ser Lys Leu Leu Asp Gly Thr Thr Ala      13

 144  TCC CGT CGC TGG ACC CGA AAG CTG GTG TTG CTC CTG CCG CCG CTG CTG     191
  14  Ser Arg Arg Trp Thr Arg Lys Leu Val Leu Leu Leu Pro Pro Leu Leu      29

 192  CTG TTC CTG TTG CGG ACC GAA TCT CTG CAA GGC TTG GAG AGT GAT GAA     239
  30  Leu Phe Leu Leu Arg Thr Glu Ser Leu Gln Gly Leu Glu Ser Asp Glu      45

 240  CGG TTC CGG ACC CGC GAA AAT GAG TGC CAC TTC TAC GCT GGT GGA CAA     287
  46  Arg Phe Arg Thr Arg Glu Asn Glu Cys His Phe Tyr Ala Gly Gly Gln      61

 288  GTG TAC CCC GGG GAG GCG TCC CGG GTT TCA GTC GCG GAT CAC TCC CTG     335
  62  Val Tyr Pro Gly Glu Ala Ser Arg Val Ser Val Ala Asp His Ser Leu      77

 336  CAT CTA AGC AAA GCC AAG ATC TCC AAG CCA GCA CCT TAT TGG GAA GGA     383
  78  His Leu Ser Lys Ala Lys Ile Ser Lys Pro Ala Pro Tyr Trp Glu Gly      93

 384  ACA GCT GTG ATT AAC GGA GAA TTC AAG GAG CTC AAA CTG ACT GAC TAT     431
  94  Thr Ala Val Ile Asn Gly Glu Phe Lys Glu Leu Lys Leu Thr Asp Tyr     109

 432  CGT GGG AAA TAC TTG GTT TTT TTC TTC TAC CCA CTG GAT TTC ACC TTT     479
 110  Arg Gly Lys Tyr Leu Val Phe Phe Phe Tyr Pro Leu Asp Phe Thr Phe     125

 480  GTG TGT CCA ACT GAA ATC ATC GCT TTT GGG GAT CGA ATT GAA GAA TTC     527
 126  Val Cys Pro Thr Glu Ile Ile Ala Phe Gly Asp Arg Ile Glu Glu Phe     141

 528  AAA TCT ATA AAT ACT GAA GTG GTA GCA TGC TCT GTT GAC TCT CAG TTT     575
 142  Lys Ser Ile Asn Thr Glu Val Val Ala Cys Ser Val Asp Ser Gln Phe     157

 576  ACT CAC TTG GCC TGG ATT AAT ACC CCT CGA AGA CAA GGA GGA CTG GGG     623
 158  Thr His Leu Ala Trp Ile Asn Thr Pro Arg Arg Gln Gly Gly Leu Gly     173

 624  CCA ATA AGG ATT CCT CTT CTT TCT GAC CTG AAC CAT CAG ATC TCA AAG     671
 174  Pro Ile Arg Ile Pro Leu Leu Ser Asp Leu Asn His Gln Ile Ser Lys     189

 672  GAC TAC GGT GTA TAC CTT GAA GAC TCA GGA CAT ACT CTT AGA GGC CTC     719
 190  Asp Tyr Gly Val Tyr Leu Glu Asp Ser Gly His Thr Leu Arg Gly Leu     205

 720  TTT ATT ATC GAT GAC AAA GGA GTC CTG AGG CAG ATT ACT CTG AAT GAC     767
 206  Phe Ile Ile Asp Asp Lys Gly Val Leu Arg Gln Ile Thr Leu Asn Asp     221

 768  CTT CCT GTC GGA AGA TCA GTG GAC GAG ACA CTG CGT TTG GTT CAA GCC     815
 222  Leu Pro Val Gly Arg Ser Val Asp Glu Thr Leu Arg Leu Val Gln Ala     237

 816  TTC CAG TAC ACT GAC AAG CAT GGA GAA GTC TGC CCT GCT GGC TGG AAA     863
 238  Phe Gln Tyr Thr Asp Lys His Gly Glu Val Cys Pro Ala Gly Trp Lys     253

 864  CCT GGT AGT GAA ACA ATA ATC CCA GAT CCA GCT GGA AAA CTG AAG TAT     911
 254  Pro Gly Ser Glu Thr Ile Ile Pro Asp Pro Ala Gly Lys Leu Lys Tyr     269

 912  TTC GAC AAG CTA AAC TGA AAA GTA CTT CAG TTA TGA TGT TTG GAC CTT     959
 270  Phe Asp Lys Leu Asn ***                                          275

 960  CTC AAT AAA GGT CAT TGT GTT ATT ACC AAA AAA AAA AAA AA           1000
```

FIG. 2. Nucleotide and deduced amino acid sequence of mouse Prx-IV. Sequence of the predicted signal peptide is underlined. Sequence of the synthetic peptide used to raise antibody in rabbit is double-underlined. This sequence has been deposited in GenBank under accession number U96746.

lines NIH-3T3 (fibroblast) and F9 (embryonic testicular teratoma). A band at about 25 kDa was detected in the cell extracts of both lines with the peptide-specific antiserum (Fig. 5A, lanes 1 and 2), whereas the preimmune serum failed to react with any protein in the same range (data not shown). Previously, human and rat Prx-IV proteins have been reported to be secreted by Jurkat and COS-1 cells (Haridas *et al.*, 1998; Matsumoto *et al.*, 1999). However, although we could detect Prx-IV in the cell extracts of both untransfected (Fig. 5A) and pSVP4-transfected (data not shown) NIH-3T3, F9, and Jurkat (human T-lymphocyte) cells, we failed to find any Prx-IV in 3 ml of conditioned media from pSVP4-transfected NIH-3T3 or Jurkat cells (Fig. 5A, lanes 3 and 4).

We also determined the subcellular localization of Prx-IV protein in NIH-3T3 cells by confocal immunofluorescence microscopy (Fig. 5B). Prx-IV was found in the nucleus-excluded region (Fig. 5B, panel 1), consistent with a cytoplasmic and/or organellar localization. The staining was specifically erased by preincubation of the anti-Prx-IV antiserum (372-1) with the immunizing peptide (Fig. 5B, panel 2). Thus, Prx-IV is primarily an intracellular cytoplasmic peroxiredoxin.

Prx-IV prevents intracellular ROS production

As a peroxidase, Prx-IV is thought to have a function in intracellular redox. Presumably, it impacts cell signaling and gene expression through this mechanism. One redox-regulated path involves growth factor-stimulated receptor signaling (Sundaresan *et al.*, 1995; Bae *et al.*, 1997). Here, a rapid increase in intracellular ROS peaked within 5 min of stimulation of cells with platelet-derived growth factor (PDGF) or epidermal growth factor (EGF). This time course of ROS production correlated with the kinetics of the ligand-stimulated tyrosine phosphorylation. Another redox-mediated pathway related to tumor suppression is p53-induced apoptosis (Polyak *et al.*, 1997). There is ample evidence that p53-stimulated generation of intracellular ROS is critically involved in mitochondrial permeability transition (Li *et al.*, 1999), which is one of the initial events in apoptosis. To shed additional light on the intracellular antioxidant functions of mouse Prx-IV, we asked whether it might modulate EGF- and p53-induced ROS production.

EGF-stimulated generation of ROS was studied in A431 cells, which abundantly express EGF receptors (Fig. 6A). Cells transfected with pSVGal (control plasmid expressing β-galactosidase) and pSVP4 (Prx-IV-expression vector) were recognized by their reactivities with the anti-β-galactosidase and anti-Prx-IV antibodies, respectively. ROS level was measured by the DCF fluorescence. In pSVGal-transfected cells, the ROS concentration was found to increase two-fold upon stimulation with EGF. In contrast, this increase was not observed in stimulated pSVP4-transfected cells (Fig. 6A). Thus,

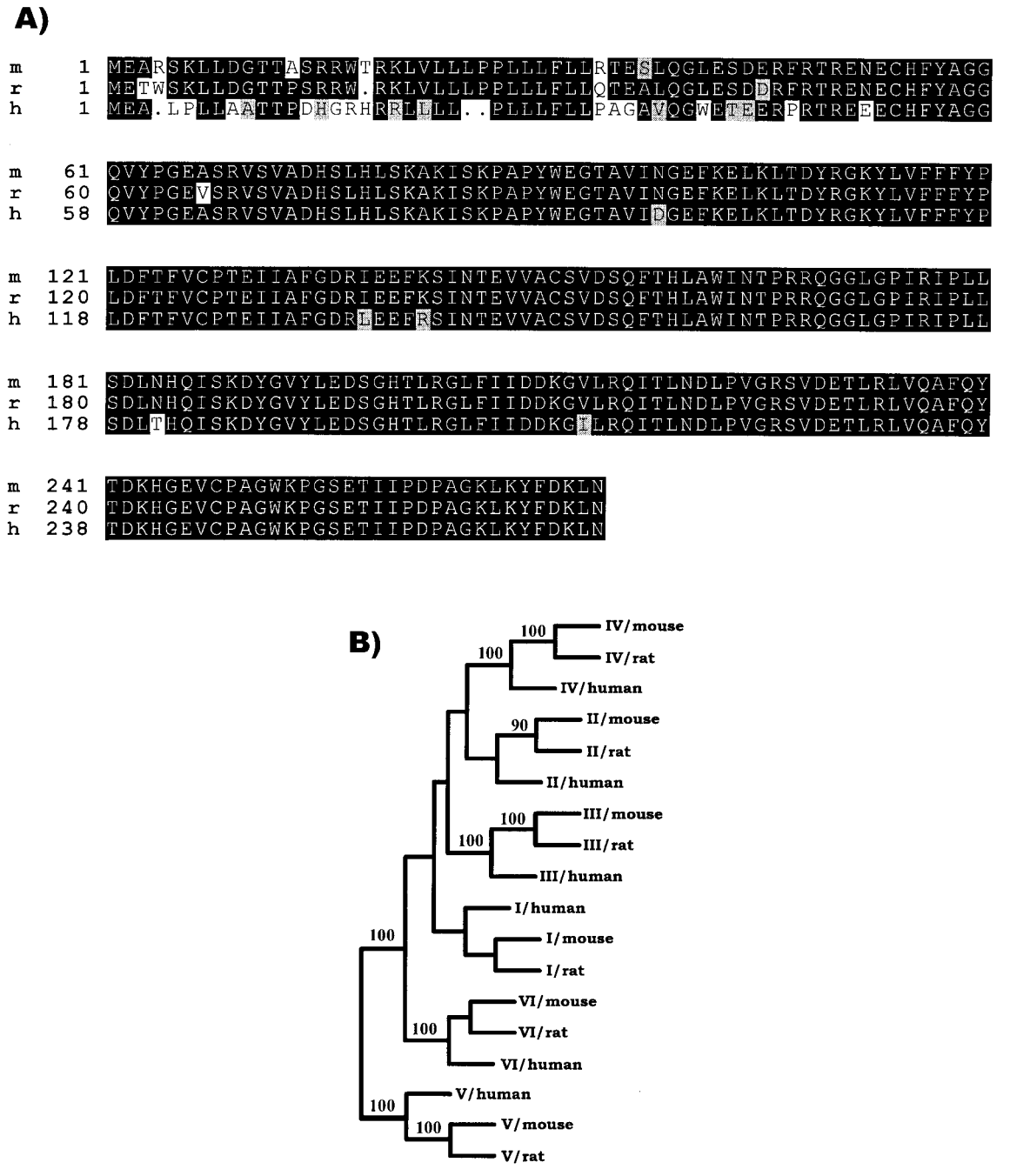

FIG. 3. Alignment and phylogenetic analysis of peroxiredoxin sequences. (**A**) Sequence alignment of mouse, rat, and human Prx-IV proteins. Identical amino acids are shown as white against black. Conservative substitutions are gray shaded. The GenBank accession numbers of human and rat Prx-IV sequences are U25182 and AF106945, respectively. (**B**) Consensus distance-matrix tree of representative peroxiredoxins. Phylogenies were inferred from protein sequences using a distance-matrix. The tree was reconstructed using the neighbor-joining algorithm. Bootstrap replication was performed and the majority rule consensus tree was generated from 100 replicates. Sequences were extracted from the GenBank and SwissProt databases.

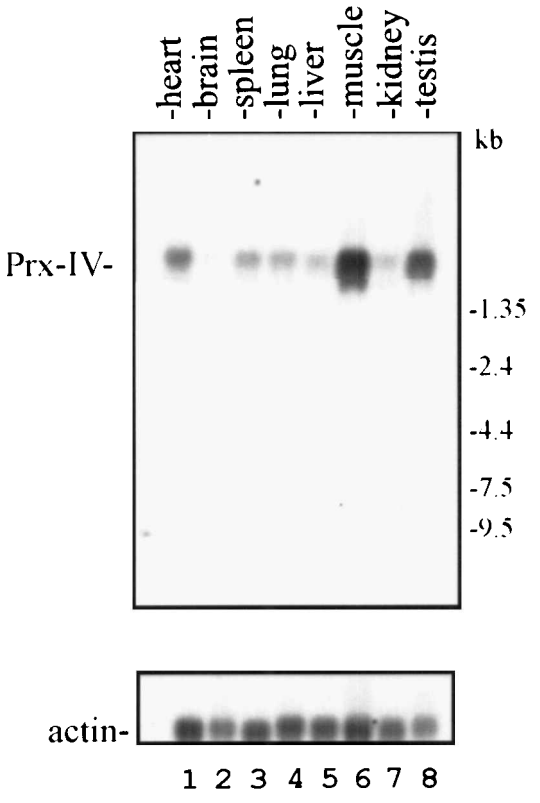

FIG. 4. Expression of mouse Prx-IV mRNA. Northern blot analysis was performed using multiple mouse tissues. Positions of the molecular weight markers are shown on the right.

overexpression of mouse Prx-IV prevented EGF-stimulated ROS production.

Next, we transfected a p53 expression plasmid (pp53) into NIH-3T3 cells and checked for ROS level. The transient expression of p53 induced a transient increase in intracellular ROS as reflected by DCF fluorescence (Fig. 6B). In p53-expressing cells, this increase was detectable within 16 hr after transfection and peaked at 24 hr. Cells were co-transfected with pp53 and pSVP4 using calcium phosphate precipitation to ensure that both plasmids were taken together into cells. DCF fluorescence at both 16 and 24 hr was significantly weaker in these co-transfected cells than that in cells which were transfected with pp53 alone. In control cells co-transfected with β-galactosidase, the DCF fluorescence did not change. These results suggest that the expression of Prx-IV counteracted the generation of intracellular ROS induced by p53.

DISCUSSION

In this study, we have identified the mouse Prx-IV cDNA (Fig. 2) through homology searching. Mouse Prx-IV is highly conserved with its human and rat orthologs (Fig. 3A). Evolutionarily Prx-IV is closer to Prx-I/-II/-III than to Prx-V/-VI (Fig. 3B). Consistent with previous mapping data in mouse and human, human Prx-IV gene localized to chromosome Xp22.135–136, is in close proximity to SAT. A BAC clone containing the complete human Prx-IV locus was also identified and characterized (Fig. 1). Mouse Prx-IV is ubiquitously expressed (Figs. 4 and 5A). However, in contrast with previous studies (Haridas *et al.*, 1998; Matsumoto *et al.*, 1999), we failed to detect Prx-IV in the conditioned media of NIH-3T3 and Jurkat cells (Fig. 5A). Mouse Prx-IV protein localized to the nucleus-excluded region of cultured NIH-3T3 cells (Fig. 5B). Inside cells, over-expression of mouse Prx-IV can prevent ROS generation stimulated by EGF and p53 (Fig. 6).

Examining the complete genomic clone of Prx-IV revealed interestingly that the whole signal peptide in human Prx-IV was encoded within the first exon (Fig. 3A). Presumably, this sorting signal may have evolved through a single discrete gain-of-function event. Further investigations will elucidate the molecular mechanisms for the transcriptional regulation and differential expression of Prx-IV gene.

Human and rat Prx-IV were previously found in Jurkat- or COS-1-conditioned media (Haridas *et al.*, 1998; Matsumoto *et al.*, 1999). Surprisingly, while transfected rat Prx-IV was previously detectable from only 10 μl of culture medium from COS-1 cells (Matsumoto *et al.*, 1999), we failed to detect Prx-IV from samples concentrated from 3 ml of either NIH-3T3- or Jurkat-conditioned media (Fig. 5A). This may suggest that extracellular secretion of protein is low. Because Prx-IV is expressed abundantly inside cells, it is difficult to rule out the possibility that the Prx-IV protein recovered from culture supernatants originated from lysed or apoptotic cells. Additionally, when we incubated U937 (histiocytic lymphoma) cells with purified recombinant Prx-IV, we failed to observe any effects on NF-κB or c-Jun N-ter-

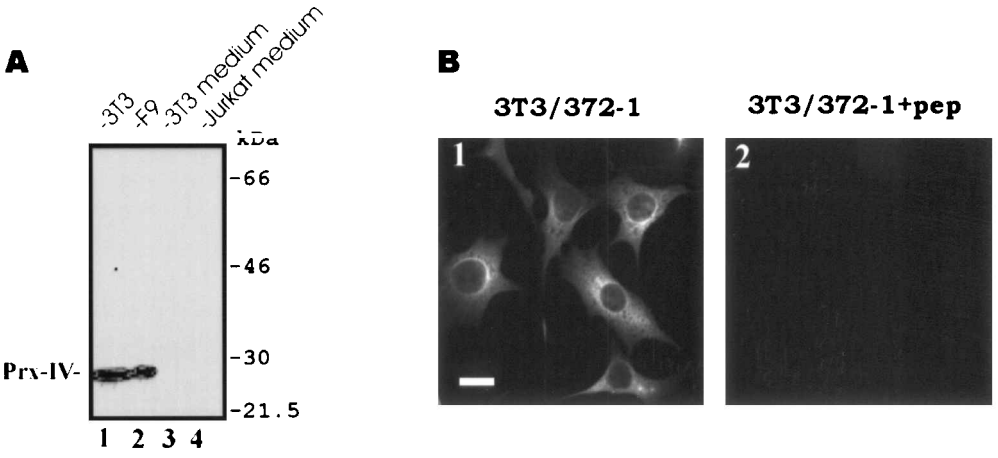

FIG. 5. Expression and subcellular localization of mouse Prx-IV protein. (**A**) Western blot analysis of Prx-IV protein in extracts of untransfected NIH-3T3 and F9 cells (lanes 1–2), and in conditioned media from pSVP4-transfected NIH-3T3 and Jurkat cells (lanes 3–4). Positions of the molecular weight markers are shown on the right. Experiments were repeated for four times with similar results. (**B**) Confocal immunofluorescence microscopy. NIH-3T3 cells were washed, fixed, and stained individually with anti-Prx-IV antibody 372-1 (panel 1) or with 372-1 pre-incubated with 5 μg of immunizing peptide (panel 2).

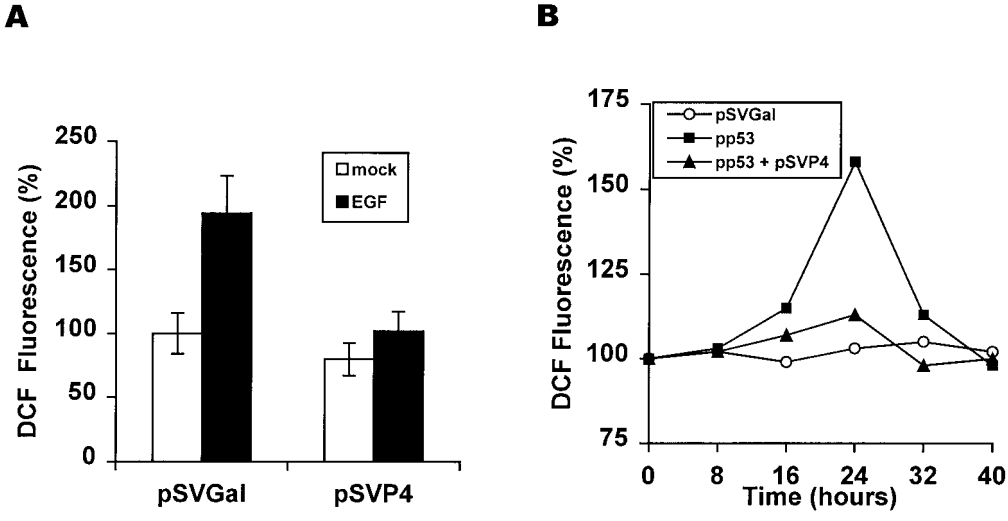

FIG. 6. Mouse Prx-IV inhibits EGF- and p53-induced ROS production. (**A**) Influence on EGF-dependent ROS production. A431 cells were transfected with control plasmid pSVGal or with pSVP4 expressing mouse Prx-IV. Transfected cells were serum-deprived for 6 hr and treated with 0.5 μg of EGF for 5 min. Fluorescent dye was then added and incubated with cells for 8 min. DCF fluorescence was measured and calculated as percentage of control (mocked-treated pSVGal-transfected cells). Results represent the average of three independent experiments and error bars indicate the standard error. DCF fluorescence data from EGF-stimulated pSVGal-transfected cells and EGF-stimulated pSVP4-transfected cells were compared by Student's *t*-test and the difference was found to be statistically significant ($p < 0.01$). (**B**) Prx-IV counteracts p53-induced generation of ROS. NIH-3T3 cells were transfected individually with the indicated plasmids (10 μg). DCF was added at the indicated time points after transfection, and the relative DCF fluorescence was calculated as percentage of control (pSVGal-transfected cells at time zero). Results are representative of three independent experiments and the standard deviation of each point is less than 10%. Data collected at 24 hr after transfection were compared by Student's *t*-test and the difference between pp53-transfected cells and cells transfected with pp53 + pSVP4 was statistically significant ($p < 0.001$). Consistent with results from A431 cells as shown in **A**, transfection of NIH-3T3 cells with pSVP4 alone also led to a slight reduction in DCF fluorescence if compared to pSVGal-transfected cells (data not shown).

minal kinase (JNK) (data not shown). Our results argue that the predominant Prx-IV activity is intracellular and that only a very small amount could be secreted to function as an extracellular cytokine.

We note that $DCFH_2$ can be oxidized by various ROS as well as reactive nitrogen species (Crow, 1997). However, stimulation of ROS production by EGF and p53 has already been documented (Bae *et al.*, 1997; Li *et al.*, 1999; Zhou *et al.*, 2000), and we believed that this stimulation could be sensitively and authentically reflected by DCF fluorescence. Here, we have provided the first evidence that Prx-IV functions as an antioxidant in mammalian cells by preventing the production of intracellular ROS (Fig. 6). Through this mechanism, Prx-IV might regulate signal transduction as related to EGF and p53, as well as other growth factors and tumor suppressor proteins. Our data propose that Prx-IV is primarily a regulator of intracellular redox.

ACKNOWLEDGMENTS

We gratefully acknowledge the Baylor College of Medicine Human Genome Sequencing Center for generating and disseminating DNA sequence and chromosomal mapping data. We thank Tony K.T. Chin, H.H. Kwok, Oscar G.W. Wong, and H.W. Wu for critically reading the manuscript, and Lan Lin for assistance in manuscript preparation. This work was supported in part by a research initiation grant (to D.-Y.J.) from the Committee on Research and Conference Grants, the University of Hong Kong and an HKU Foundation grant (to P.C.W.F.).

ABBREVIATIONS

BAC, Bacteria artificial chromosome; cDNA, complementary DNA; DCF, 2′,7′-dichlorofluorescein; EGF, epidermal growth factor; EST, expressed sequence tags; FCS, fetal calf serum; FISH, fluorescent *in situ* hybridization; JNK, c-Jun N-terminal kinase; PCR, polymerase chain reaction; PDGF, platelet-derived growth factor; Prx, peroxiredoxin; ROS, reactive oxygen species; SAT, spermidine/spermine N^1-acetyltransferase; SDS-PAGE, sodium dodecyl sulfate-polyacrylamide gel electrophoresis.

REFERENCES

ARAKI, M., NANRI, H., EJIMA, K., MURASATO, Y., FUJIWARA, T., NAKASHIMA, Y., and IKEDA, M. (1999). Antioxidant function of the mitochondrial protein SP-22 in the cardiovascular system. J. Biol. Chem. **274,** 2271–2278.

BAE, Y.S., KANG, S.W., SEO, M.S., BAINES, I.C., TEKLE, E., CHOCK, P.B., and RHEE, S.G. (1997). Epidermal growth factor (EGF)-induced generation of hydrogen peroxide: Role in EGF receptor-mediated tyrosine phosphorylation. J. Biol. Chem. **272,** 217–221.

CHA, M.-K., KIM, H.-K., and KIM, I.-H. (1995). Thioredoxin-linked "thiol peroxidase" from periplasmic space of *Escherichia coli*. J. Biol. Chem. **270,** 28635–28641.

CHA, M.-K., KIM, H.-K., and KIM, I.-H. (1996). Mutation and mutagenesis of thiol peroxidase of *Escherichia coli* and a new type of thiol peroxidase family. J. Bacteriol. **178,** 5610–5614.

CHAE, H.Z., KIM, I.-H., KIM, K., and RHEE, S.G. (1993). Cloning, sequencing, and mutation of thiol-specific antioxidant gene of *Saccharomyces cerevisiae*. J. Biol. Chem. **268,** 16815–16821.

CHAE, H.Z., CHUNG, S.J., and RHEE, S.G. (1994a). Thioredoxin-dependent peroxide reductase from yeast. J. Biol. Chem. **269,** 27670–27678.

CHAE, H.Z., ROBISON, K., POOLE, L.B., CHURCH, G., STORZ, G., and RHEE, S.G. (1994b). Cloning and sequencing of thiol-specific antioxidant from mammalian brain: alkyl hydroperoxide reductase and thiol-specific antioxidant define a large family of antioxidant enzymes. Proc. Natl. Acad. Sci. USA **91,** 7017–7021.

CHOI, H.-J., KANG, S.W., YANG, C.-H., RHEE, S.G., and RYU, S.-E. (1998). Crystal structure of a novel human peroxidase enzyme at 2.0 angstrom resolution. Nature Struct. Biol. **5,** 400–406.

CROW, J.P. (1997). Dichlorodihydrofluorescein and dihydrorhodamine 123 are sensitive indicators of peroxynitrite *in vitro*: implications for intracellular measurement of reactive nitrogen and oxygen species. Nitric Oxide **1,** 145–157.

FELSENSTEIN, J. (1996). Inferring phylogenies from protein sequences by parsimony, distance and likelihood methods. Methods Enzymol. **266,** 418–427.

FISHER, A.B., DODIA, C., MANEVICH, Y., CHEN, J.-W., and FEINSTEIN, S.I. (1999). Phospholipid hydroperoxides are substrates for non-selenium glutathione peroxidase. J. Biol. Chem. **274,** 21326–21334.

FRANK, S., MUNZ, B., and WERNER, S. (1997). The human homologue of a bovine non-selenium glutathione peroxidase is a novel keratinocyte growth factor-regulated gene. Oncogene **14,** 915–921.

HARIDAS, V., NI, J., MEAGER, A., SU, J., YU, G.-L.,

ZHAI, Y., KYAW, H., AKAMA, K.T., HU, J., VAN ELDIK, L.J., and AGGARWAL, B.B. (1998). TRANK, a novel cytokine that activates NF-κB and c-Jun N-terminal kinase. J. Immunol. **161,** 1–6.

HIROTSU, S., ABE, Y., OKADA, K., NAGAHARA, N., HORI, H., NISHINO, T., and HAKOSHIMA, T. (1999). Crystal structure of a multifunctional 2-Cys peroxiredoxin heme-binding protein 23 kDa/proliferation-associated gene product. Proc. Natl. Acad. Sci. USA **96,** 12333–12338.

ICHIMIYA, S., DAVIS, J.G., O'ROURKE, D.M., KATSUMATA, M., and GREENE, M.I. (1997). Murine thioredoxin peroxidase delays neuronal apoptosis and is expressed in areas of the brain most susceptible to hypoxic and ischemic injury. DNA Cell. Biol. **16,** 311–321.

JEONG, J.S., KWON, S.J., KANG, S.W., RHEE, S.G., and KIM, K. (1999). Purification and characterization of a second type thioredoxin peroxidase (type II TPx) from *Saccharomyces cerevisiae*. Biochemistry **38,** 776–783.

JIN, D.-Y., and JEANG, K.-T. (2000). Peroxiredoxins in cell signaling and HIV infection. In: *Antioxidant and Redox Regulation of Genes*. C.K. Sen, H. Siers, and P.A. Baeuerle, eds. (Academic Press, San Diego, CA) pp. 381–407.

JIN, D.-Y., CHAE, H. Z., RHEE, S.G., and JEANG, K.-T. (1997). Regulatory role for a novel human thioredoxin peroxidase in NF-κB activation. J. Biol. Chem. **272,** 30952–30961.

JIN, D.-Y., SPENCER, F., and JEANG, K.-T. (1998). Human T cell leukemia virus type 1 oncoprotein Tax targets the human mitotic checkpoint protein MAD1. Cell **93,** 81–91.

KANG, S.W., BAINES, I.C., and RHEE, S.G. (1998a). Characterization of a mammalian peroxiredoxin that contains one conserved cysteine. J. Biol. Chem. **273,** 6303–6311.

KANG, S.W., CHAE, H.Z., SEO, M.S., KIM, K., BAINES, I.C., and RHEE, S.G. (1998b). Mammalian peroxiredoxin isoforms can reduce hydrogen peroxide generated in response to growth factors and tumor necrosis factor-α. J. Biol. Chem. **273,** 6297–6302.

KERN, S.E., KINZLER, K.W., BRUSKIN, A., JAROSZ, D., FRIEDMAN, P., PRIVES, C., and VOGELSTEIN, B. (1991). Identification of p53 as a sequence-specific DNA-binding protein. Science **252,** 1708–1711.

KNOOPS, B., CLIPPE, A., BOGARD, C., ARSALANE, K., WATTIEZ, R., HERMANS, C., DUCONSEILLE, E., FALMAGNE, P., and BERNARD, A. (1999). Cloning and characterization of AOEB166, a novel mammalian antioxidant enzyme of the peroxiredoxin family. J. Biol. Chem. **274,** 30451–30458.

KOWALTOWSKI, A.J., NETTO, L.E., and VERCESI, A.E. (1998). The thiol-specific antioxidant enzyme prevents mitochondrial permeability transition: Evidence for the participation of reactive oxygen species in this mechanism. J. Biol. Chem. **273,** 12766–12769.

KROPOTOV, A., SEDOVA, V., IVANOV, V., SAZEEVA, N., TOMILIN, A., KRUTILINA, R., OEI, S.L., GRIESENBECK, J., BUCHLOW, G., and TOMILIN, N. (1999). A novel human DNA-binding protein with sequence similarity to a subfamily of redox proteins which is able to repress RNA-polymerase-III-driven transcription of the Alu-family retroposons in vitro. Eur. J. Biochem. **260,** 336–346.

LEE, J., SPECTOR, D., GODON, C., LABARRE, J., and TOLEDANO, M.B. (1999). A new antioxidant with alkyl hydroperoxide defense properties in yeast. J. Biol. Chem. **274,** 4537–4544.

LI, P.-F., DIETZ, R., and VON HARSDORF, R. (1999). p53 regulates mitochondrial membrane potential through reactive oxygen species and induces cytochrome c-independent apoptosis blocked by bcl-2. EMBO J. **18,** 6027–6036.

LIM, M.J., CHAE, H.Z., RHEE, S.G., YU, D.-Y., LEE, K.-K., and YEOM, Y.I. (1998). The type II peroxiredoxin gene family of the mouse: molecular structure, expression and evolution. Gene **216,** 197–205.

LYU, M.S., RHEE, S.R., CHAE, H.Z., LEE, T.H., ADAMSON, M.C., KANG, S.W., JIN, D.-Y., JEANG, K.-T., and KOZAK, C.A. (1999). Genetic mapping of six mouse peroxiredoxin genes and fourteen peroxiredoxin related sequences. Mamm. Genome **10,** 1017–1019.

MATSUMOTO, A., OKADO, A., FUJII, T., FUJII, J., EGASHIRA, M., NIIKAWA, N., and TANIGUCHI, N. (1999). Cloning of the peroxiredoxin gene family in rats and characterization of the fourth member. FEBS Lett. **443,** 246–250.

MONTEMARTINI, M., NOGOCEKE, E., SINGH, M., STEINERT, P., FLOHE, L., and KALISZ, H.M. (1998). Sequence analysis of the tryparedoxin peroxidase gene from *Crithidia fasciculata* and its functional expression in *Escherichia coli*. J. Biol. Chem. **273,** 4864–4871.

POLYAK, K., XIA, Y., ZWEIER, J.L., KINZLER, K.W., and VOGELSTEIN, B. (1997). A model for p53-induced apoptosis. Nature **389,** 300–305.

SARAFIAN, T.A., VERITY, M.A., VINTERS, H.V., SHIH, C.C.-Y., SHI, L., JI, X.D., DONG, L., and SHAU, H. (1999). Differential expression of peroxiredoxin subtypes in human brain cell types. J. Neurosci. Res. **56,** 206–212.

SINGH, A.K., and SHICHI, H. (1998). A novel glutathione peroxidase in bovine eye: Sequence analysis, mRNA level, and translation. J. Biol. Chem. **273,** 26171–26178.

SUNDARESAN, M., YU, Z.-X., FERRANS, V.J., IRANI, K., and FINKEL, T. (1995). Requirement for generation of H_2O_2 for platelet-derived growth factor signal transduction. Science **270,** 296–299.

VERDOUCQ, L., VIGNOLS, F., JACQUOT, J.P., CHARTIER, Y., and MEYER, Y. (1999). *In vivo* characterization of a thioredoxin h target protein defines a new peroxiredoxin family. J. Biol. Chem. **274,** 19714–19722.

WAN, X.-Y., ZHOU, Y., YAN, Z.-Y., WANG, H.-L., HOU, Y.-D., and JIN, D.-Y. (1997). Scavengase p20: a novel family of bacterial antioxidant enzymes. FEBS Lett. **407,** 32–36.

YAMASHITA, H., AVRAHAM, S., JIANG, S., LONDON,

R., VAN VELDHOVEN, P.P., SUBRAMANI, S., ROGERS, R.A., and AVRAHAM, H. (1999). Characterization of human and murine PMP20 peroxisomal proteins that exhibit antioxidant activity *in vitro*. J. Biol. Chem. **274,** 29897–29904.

ZHANG, P., LIU, B., KANG, S.W., SEO, M.S., RHEE, S.G., and OBEID, L.M. (1997). Thioredoxin peroxidase is a novel inhibitor of apoptosis with a mechanism distinct from that of Bcl-2. J. Biol. Chem. **272,** 30615–30618.

ZHOU, Y., WAN, X.-Y., WANG, H.-L., YAN, Z.-Y., HOU, Y.-D., and JIN, D.-Y. (1997). Bacterial scavengase p20 is structurally and functionally related to peroxiredoxins. Biochem. Biophys. Res. Commun. **233,** 848–852.

ZHOU, Y., KOK, K.H., CHUN, A.C.S., WONG, C.M., WU, H.W., LIN, M.C.M., FUNG, P.C.W., KUNG, H.-F., and JIN, D.-Y. (2000). Mouse peroxiredoxin V is a thioredoxin peroxidase that inhibits p53-induced apoptosis. Biochem. Biophys. Res. Commun. **268,** 921–927.

Address reprint requests to:
Dr. Dong-Yan Jin
Institute of Molecular Biology
The University of Hong Kong
8/F Kadoorie Biological Sciences Building
Pokfulam Road, Hong Kong

E-mail: dyjin@hkucc.hku.hk

Received for publication February 7, 2000; accepted May 9, 2000.